Superconductivity in Magnesium Diboride

Miles Wu (Advisor: Prof. Ong)

May 6, 2011

Abstract

A few important basic properties of superconductivity are introduced. The microscopic BCS theory is derived using two different methods: the variational approach and the quasiparticle approach. Various thermodynamic quantiaties are computed such as the heat capacity and free energy. These are then illustrated using data from Aluminium. Ginzburg–Landau theory is then introduced for the purpose of finding the upper critical field in Type II superconductors. We use both theories to analyse experimental data from Magnesium Diboride. We find that there is evidence for two energy gaps and we calculate their values with a curve fitting approach.

Contents

1 Introduction

Superconductivity is a phenomenon that occurs at low temperatures in certain materials, where the electrical resistance completely disappears. There is a certain critical temperature, T_c, which depends on the material, that serves as the phrase transition point. Below this temperature superconductivity occurs; above it, it ceases.

Another important characteristic of superconductivity is the Meissner effect. This is where superconductors exhibit perfect diamagnetism and all the magnetic flux is expelled. Whilst perfect conductivity would explain how applied magnetic fields are prevented from entering the superconductor (as the magnetic field is applied, it would induce an emf, whose current would generate a magnetic field exactly opposite in magnitude and direction to cancel the applied field), it can not expain how a field that was already present when the material was normal is expelled when it is cooled below the critical temperature T_c. In this situation, perfect conductivity would tend to preserve the existing field via Lens' Law.

It was also found that if a very strong magnetic field were applied, superconductivity would be lost. The field strength at which this occurs is termed the critical field, H_c, and it is dependent on temperature.

In this paper, we introduce and examine two important theories that are used to explain superconductivity. BCS theory is a microscopic description of superconductivity that involves quantum mechnical arguments relating to the electrons. By comparing the predictions of certain parameters from the theory to actual data from experiments on superconducting Aluminium, we attempt to show its validity and accuracy. Ginzburg-Landau theory is a phenomological macroscopic theory that helps in explaining certain types of superconductors (Type II superconductors).

Magnesium diboride (MgB_2) is a recently discovered Type II superconductor. We examine experimental data taken on MgB_2 to see if the model in BCS theory is sufficient to understand the behaviour of superconducting MgB_2.

2 BCS Theory

2.1 Cooper Pairs

The discovery in 1950 that the critical temperature, T_c, of a superconductor changed if a different isotope was used provided a crucial piece of evidence that was critical in the synthesis of BCS theory [7]. The change in mass between different isotopes only affects the lattice vibration frequencies, and does not change anything about the charge distribution or the electrons themselves. Different isotopes having different critical temperatures suggested that the lattice was somehow involved in superconductivity.

Cooper in 1956 showed that an attractive force between electrons in a Fermi sea would cause at least one pair to enter a bound state together with a lower energy [4]. He proved that this would occur regardless of how small this attractive force was, so long as it was attractive. Whilst this was an important step towards understanding superconductivity, a couple of important questions remained. The origin of this attractive force was unknown, especially when it was thought to be completely dwarfed and negated by the Couloumb repulsion between the two electrons. Cooper also only showed that a single pair would be formed, not the many pairs required for superconductivity.

Putting these two pieces of evidence together, the attraction comes from electron-phonon interactions (phonons are the quasiparticle of lattice vibrations) [1, p.56]. Consider a single electron

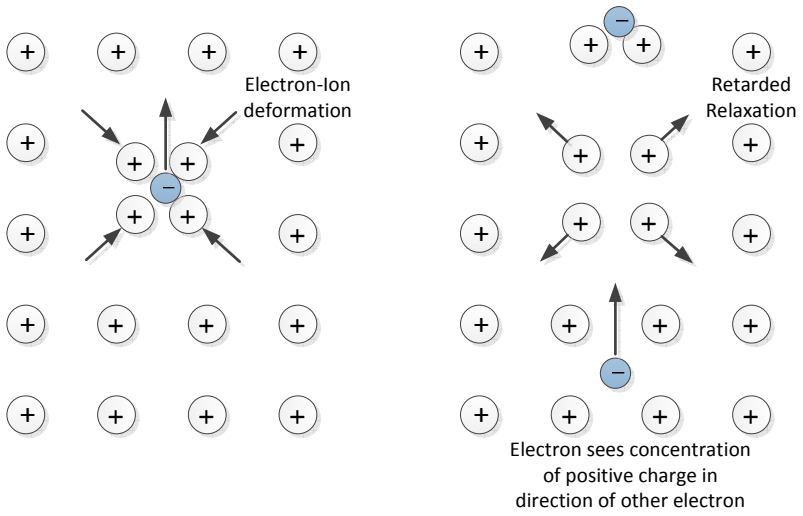

Figure 1: The left pane shows the lattice deformation (phonon) caused by the electron. The right pane shows that that whilst the first electron is no longer present nearby, the deformation has not fully relaxed yet, and the second electron sees this concentrated region of positive charge and is attracted to it. Whilst it is not attracted to the other electron *per se*, it has an effective attraction since it is in the correct direction. This is the electron-phonon interaction that causes Cooper pairing.

moving through a lattice of postively charged ions. As it passes through the lattice, the positive ions are electrostatically attracted towards it, causing a deformation in the lattice. Once the electron moves away, the deformation relaxes, but because the ions are several orders of magnitude heavier than the electron, they take a significant amount of time to relax. In the mean time, another electron sees the increased concentration of positive charge due to the deformation that has not fully relaxed yet, and therefore it feels an attractive force in the direction of the first electron. Even though there is no direct attraction between the two electrons, via the lattice there is an effective attraction which can outweigh the Coulomb repulsion, leading to the net attraction that is needed for Cooper pairs. This electron-phonon interaction is shown in Figure 1.

Metals that are poor conductors tend to become superconductors at low temperatures and those that are conductors do not [1, p.58]. This is opposite to what might be expected initially as good conductors are closer to becoming perfect ones. However, in good conductors the electron-phonon interaction is weak as exhibited by the low resistance-causing scattering, so the attractive force needed for Cooper pairs is outweighed by the Coulomb repulsion, and superconductivity does not occur.

2.2 Ground State

In second quantization, the wavefunction representing N electrons is written as a sequence of creation operators operating on the vacuum state: $|\psi\rangle = c^\dagger_{\mathbf{k1},s1} c^\dagger_{\mathbf{k2},s2} c^\dagger_{\mathbf{k3},s3} \ldots |0\rangle$. Because of Cooper pairs, all the electrons are paired with another electron of opposite spin and momentum. This allows the wavefunction to be written as $|\psi\rangle = \prod_{\text{occupied}} (c^\dagger_{\mathbf{k_i},\uparrow} c^\dagger_{-\mathbf{k_i},\downarrow})|0\rangle$, which represents a state where each paired state of momentum is either empty or occupied by two electrons.

For the BCS ground state, we consider a situation where each paired state is not definitely occupied or empty, but instead has a probability $|v_{\mathbf{k}}|^2$ of being filled and probability $|u_{\mathbf{k}}|^2$ of being empty [9, p.1]. Obviously the two probabilities must add up to one, i.e. $|v_{\mathbf{k}}|^2 + |u_{\mathbf{k}}|^2 = 1$. The BCS ground state wavefunction is therefore:

$$|\psi\rangle = \prod_{\mathbf{k}} (u_{\mathbf{k}} + v_{\mathbf{k}} c^{\dagger}_{\mathbf{k},\uparrow} c^{\dagger}_{-\mathbf{k},\downarrow})|0\rangle. \tag{1}$$

2.3 The BCS Approximation

The general Hamiltonian for an electron gas is [9, p.1]:

$$\mathcal{H} = \sum_{\mathbf{k},s} \xi_{\mathbf{k}} c^{\dagger}_{\mathbf{k},s} c_{\mathbf{k},s} + \frac{1}{2} \sum_{\mathbf{k},\mathbf{k}',s,s',\mathbf{q}} V(\mathbf{q}) c^{\dagger}_{\mathbf{k}+\mathbf{q},s} c^{\dagger}_{\mathbf{k}'-\mathbf{q},s'} c_{\mathbf{k}',s'} c_{\mathbf{k},s}. \tag{2}$$

This Hamiltonian uses creation ($c^{\dagger}$) and annihilation (c) operators from second quantization field theory. First we must state a few important properties of these operators. They form a conjucated pair, i.e. $c^{\dagger} = c^*$. The annihilation operator removes an electron with specified momentum from the field. If one does not exist then the operator yields zero. Likewise, the creation operator creates an electron with specified momentum from the field. If one already exists, by the Pauli exclusion principle we cannot have another, so it yields zero. Finally, in order for an expectation value to be unity, all the creation and annihilation operators must be balanced (an equal number of $c^{\dagger}_{\mathbf{k}}$ and $c_{\mathbf{k}}$ terms).

The first term corresponds to the kinetic energy of the electrons measured with reference to the chemical potential, i.e. $\xi_{\mathbf{k}} = \epsilon_{\mathbf{k}} - \mu$. The pair of the construction and annihilation operator together is known as the number operator, because it picks out either zero or one depending on whether the state is occupied or not. As the kinetic energies $\xi_{\mathbf{k}}$ are summed over all the possible momentums, the number operator ensures that only those states that are occupied are counted.

The second term is a more complex interaction term that deals with the scattering of a pair of electrons from the ($\mathbf{k}$, $\mathbf{k}'$) state to the ($\mathbf{k}+\mathbf{q}$, $\mathbf{k}'-\mathbf{q}$) state. As it is summed over all possible states, every pair is counted twice and the factor $1/2$ compensates for this. The two annihilation operators ensure that the two electrons with $\mathbf{k}$ and $\mathbf{k}'$ momentum exist, and the two construction operators ensure that the $\mathbf{k}+\mathbf{q}$ and $\mathbf{k}'-\mathbf{q}$ states are currently unoccupied so that there is a vacancy for the scattered electrons (the Pauli exclusion principle only allows one per state).

The Hamiltonian in Equation (2) is excedingly complex, as it involves interactions between every combination of two electrons. This is of the order of N^2 interaction terms. In BCS theory we simplify this interaction term by only considering pair-wise interactions, where $\mathbf{k} = \mathbf{k}'$, reducing it to merely N terms [9, p.1]. By the Pauli exclusion principle the scattering must therefore be from ($\mathbf{q}\uparrow$, $-\mathbf{q}\downarrow$) to ($\mathbf{k}\uparrow$, $-\mathbf{k}\downarrow$). The reduced Hamiltonian is now:

$$\mathcal{H} = \sum_{\mathbf{k},s} \xi_{\mathbf{k}} c^{\dagger}_{\mathbf{k},s} c_{\mathbf{k},s} + \frac{1}{2} \sum_{\mathbf{k},\mathbf{q}} V_{\mathbf{k}\mathbf{q}} c^{\dagger}_{\mathbf{k}\uparrow} c^{\dagger}_{-\mathbf{k}\downarrow} c_{-\mathbf{q}\downarrow} c_{\mathbf{q}\uparrow}. \tag{3}$$

2.4 Variational Approach

The general approach behind the variational approach is to calculate an expression for the energy and to take the derivative of this to find the minimum. The following derivation follows that given

by Ong [9]. First of all we calculate the energy of the system, where ψ is that from Equation (1):

$$E = \langle\psi| \sum_{\mathbf{k},s} \xi_{\mathbf{k}} c^\dagger_{\mathbf{k},s} c_{\mathbf{k},s} + \frac{1}{2} \sum_{\mathbf{k},\mathbf{q}} V_{\mathbf{kq}} c^\dagger_{\mathbf{q}\uparrow} c^\dagger_{-\mathbf{q}\downarrow} c_{-\mathbf{k}\downarrow} c_{\mathbf{k}\uparrow} |\psi\rangle. \tag{4}$$

Looking at the kinetic energy term first,

$$T = \sum_{\mathbf{k},s} \xi_{\mathbf{k}} \sum_{\mathbf{q},\mathbf{p}} \langle 0|(u^*_{\mathbf{q}} + v^*_{\mathbf{q}} c_{\mathbf{q}\uparrow} c_{-\mathbf{q}\downarrow}) c^\dagger_{\mathbf{k},s} c_{\mathbf{k},s} (u_{\mathbf{p}} + v_{\mathbf{p}} c^\dagger_{\mathbf{p}\uparrow} c^\dagger_{-\mathbf{p}\downarrow})|0\rangle, \tag{5}$$

we see that the cross terms involving $u^*_{\mathbf{q}} v_{\mathbf{p}}$ and $v^*_{\mathbf{q}} u_{\mathbf{p}}$ are zero because then the creation and annihilation operators would not be balanced. The $u^*_{\mathbf{q}} c^\dagger_{\mathbf{k},s} c_{\mathbf{k},s} u_{\mathbf{p}}$ term also cancels because the annihilation term meets the vacuum and yields zero. This leaves us with the $v^*_{\mathbf{q}} v_{\mathbf{p}} \langle 0| c_{\mathbf{q}\uparrow} c_{-\mathbf{q}\downarrow} c^\dagger_{\mathbf{k},s} c_{\mathbf{k},s} c^\dagger_{\mathbf{p}\uparrow} c^\dagger_{-\mathbf{p}\downarrow} |0\rangle$ term.

To unravel this string of operators, we examine them in the order they are applied (from the right). First $c^\dagger_{\mathbf{p}\uparrow} c^\dagger_{-\mathbf{p}\downarrow}$ creates a pair of electrons with momentum $\pm\mathbf{p}$. Next $c_{\mathbf{k},s}$ annhilates an electron with momentum $\mathbf{k}$ and immediately it is recreated by $c^\dagger_{\mathbf{k},s}$. For the non-zero terms, we must have $\mathbf{k} = \mathbf{p}$ and $s =\uparrow$, or $\mathbf{k} = -\mathbf{p}$ and $s =\downarrow$, because otherwise the annihilation operator would yield zero as there would be no electron with momentum $\pm\mathbf{k}$ to destroy. To preserve overall balance, we must have $\mathbf{q} = \mathbf{p}$ too. Therefore we are now left with:

$$T = \sum_{\mathbf{k},s} \xi_{\mathbf{k}} v^*_{\mathbf{k}} v_{\mathbf{k}} = \sum_{\mathbf{k}} 2\xi_{\mathbf{k}} |v_{\mathbf{k}}|^2. \tag{6}$$

We now proceed to do the same thing for the interaction term. First of all, let us introduce the pair creation and annihilation operators:

$$b^\dagger_{\mathbf{k}} = c^\dagger_{\mathbf{k}\uparrow} c^\dagger_{-\mathbf{k}\downarrow}, \qquad b_{\mathbf{k}} = c_{\mathbf{k}\uparrow} c_{-\mathbf{k}\downarrow}. \tag{7}$$

These just simplify the algebra. Like earlier because the creation and annihilation operators must be balanced, we know that the momentum states in the left bra must match the middle and the right ket. Therefore we can remove one of sumations, and our interaction term simplifies to:

$$V = \sum_{\mathbf{k},\mathbf{q}} V_{\mathbf{kq}} \langle 0|(u^*_{\mathbf{k}} + v^*_{\mathbf{k}} b_{\mathbf{k}})(u^*_{\mathbf{q}} + v^*_{\mathbf{q}} b_{\mathbf{q}}) b^\dagger_{\mathbf{k}} b_{\mathbf{q}} (u_{\mathbf{q}} + v_{\mathbf{q}} b^\dagger_{\mathbf{q}})(u_{\mathbf{k}} + v_{\mathbf{k}} b^\dagger_{\mathbf{k}})|0\rangle. \tag{8}$$

If we look at the middle two operators, $b^\dagger_{\mathbf{k}} b_{\mathbf{q}}$, these create a pair with momentum $\mathbf{k}$ and destroy a pair with momentum $\mathbf{q}$. In order for this to be possible originally the $\mathbf{q}$ state must be occupied and the $\mathbf{k}$ state must be empty. After the interaction, the reverse is true. This corresponds to a amplitude of $u^*_{\mathbf{q}} v^*_{\mathbf{k}} u_{\mathbf{k}} v_{\mathbf{q}}$. Therefore, we find that:

$$V = \sum_{\mathbf{k},\mathbf{q}} V_{\mathbf{kq}} u^*_{\mathbf{q}} v^*_{\mathbf{k}} u_{\mathbf{k}} v_{\mathbf{q}}. \tag{9}$$

The total energy needs to be minimized subject to the previously mentioned constraint ($|u_{\mathbf{k}}|^2 + |v_{\mathbf{k}}|^2 = 1$). If we assume that both $u_{\mathbf{k}}$ and $v_{\mathbf{k}}$ are real, then we can introduce a new parameter $\theta_{\mathbf{k}}$ where:

$$u_{\mathbf{k}} = \sin\theta_{\mathbf{k}}, \qquad v_{\mathbf{k}} = \cos\theta_{\mathbf{k}}. \tag{10}$$

The total energy is therefore now:

$$E = T + V = \sum_{\mathbf{k}} 2\xi_{\mathbf{k}} \cos^2\theta_{\mathbf{k}} + \sum_{\mathbf{k},\mathbf{q}} V_{\mathbf{kq}} \sin\theta_{\mathbf{k}} \cos\theta_{\mathbf{q}} \sin\theta_{\mathbf{q}} \cos\theta_{\mathbf{k}}, \tag{11}$$

$$= \sum_{\mathbf{k}} \xi_{\mathbf{k}}(1 + \cos 2\theta_{\mathbf{k}}) + \sum_{\mathbf{k},\mathbf{q}} \frac{V_{\mathbf{kq}}}{4} \sin 2\theta_{\mathbf{k}} \sin 2\theta_{\mathbf{q}}. \tag{12}$$

Taking the derivative with respect to $\theta_{\mathbf{k}}$ and setting it to zero to find the minimum, we obtain (the extra factor of 2 in Equation (14) is because $\mathbf{k}$ and $\mathbf{q}$ run over the same states and so everything is counted twice):

$$\frac{\partial E}{\partial \theta_{\mathbf{k}}} = \sum_{\mathbf{k}} -2\xi_{\mathbf{k}} \sin 2\theta_{\mathbf{k}} + \sum_{\mathbf{k},\mathbf{q}} \frac{V_{\mathbf{kq}}}{2} \cos 2\theta_{\mathbf{k}} \sin 2\theta_{\mathbf{q}} = 0, \tag{13}$$

$$\tan 2\theta_{\mathbf{k}} = \frac{\sum_{\mathbf{q}} V_{\mathbf{kq}} \sin 2\theta_{\mathbf{q}}}{2\xi_{\mathbf{k}}}. \tag{14}$$

Finally, we make one more simplification about the interaction, by saying that the potential is simply a negative constant (negative is attractive), rather than trying to model the phonon interactions; in other words $V_{\mathbf{kq}} = -V$. Trying to model the electron-phonon interactions would be incredibly involved and would necessitate knowledge about the specific material's lattice structure, not leading us to a general theory. We also now introduce two new quantities to simply the algebra, whose meaning will become obvious later:

$$\Delta = \sum_{\mathbf{q}} V u_{\mathbf{q}} v_{\mathbf{q}} = \frac{1}{2} \sum_{\mathbf{q}} V \sin 2\theta_{\mathbf{q}}, \qquad E_{\mathbf{k}} = \sqrt{\Delta^2 + \xi_{\mathbf{k}}^2}. \tag{15}$$

With this, we find the following solutions satisfy Equation (14):

$$2u_{\mathbf{k}} v_{\mathbf{k}} = \sin 2\theta_{\mathbf{k}} = \frac{\Delta}{E_{\mathbf{k}}}, \qquad v_{\mathbf{k}}^2 - u_{\mathbf{k}}^2 = \cos 2\theta_{\mathbf{k}} = -\frac{\xi_{\mathbf{k}}}{E_{\mathbf{k}}}. \tag{16}$$

Using our constraint that $v_{\mathbf{k}}^2 + u_{\mathbf{k}}^2 = 1$, we find:

$$u_{\mathbf{k}}^2 = \frac{1}{2}\left(1 + \frac{\xi_{\mathbf{k}}}{E_{\mathbf{k}}}\right), \qquad v_{\mathbf{k}}^2 = \frac{1}{2}\left(1 - \frac{\xi_{\mathbf{k}}}{E_{\mathbf{k}}}\right). \tag{17}$$

Finally, we can substitute Equation (17) into our definition of Δ in Equation (15):

$$\Delta = \frac{V}{2} \sum_{\mathbf{k}} \sqrt{1 - \frac{\xi_{\mathbf{k}}^2}{E_{\mathbf{k}}^2}} = \frac{V}{2} \sum_{\mathbf{k}} \frac{\Delta}{E_{\mathbf{k}}}. \tag{18}$$

We convert the sum over all the $\mathbf{k}$ momentum states into an integral by using the density of states $N(0)$. In the Debye approximation model of phonons, the phonons have frequencies between $\pm\omega_D$. Since the electron-phonon interactions are what create the Cooper pairing, it seems reasonable to restrict this integral to the $\pm\hbar\omega_D$ range. By cancelling Δ from both sides we obtain the following self-consistency condition:

$$N(0)V \int_{-\hbar\omega_D}^{\hbar\omega_D} \frac{d\xi}{\sqrt{\Delta^2 + \xi^2}} = N(0)V \sinh^{-1}\frac{\hbar\omega_D}{\Delta} = 1. \tag{19}$$

Usually we operate in a weak-coupling regime, where $N(0)V \ll 1$. Here we have $\sinh(1/N(0)V) \approx e^{1/N(0)V}/2$. Therefore we find:

$$\Delta = 2\hbar\omega_D e^{-1/N(0)V}. \tag{20}$$

2.5 Quasiparticle Approach

Whilst the variational approach outlined above was the method that was used in the original BCS paper, it is only applicable with the ground state and is not easily extended to excited states. For non-zero temperatures we need to look towards a different derivation. The following derivation follows that given by Tinkham [13, p.59].

Recall the pair creation and annihilation operators, $b_{\mathbf{k}}^{\dagger}$ and $b_{\mathbf{k}}$, as defined in Equation (7). If we use these in Equation (3), our expression for the reduced Hamiltonian, we get:

$$\mathcal{H} = \sum_{\mathbf{k},s} \xi_{\mathbf{k}} c_{\mathbf{k},s}^{\dagger} c_{\mathbf{k},s} + \frac{1}{2} \sum_{\mathbf{k},\mathbf{q}} V_{\mathbf{kq}} (c_{\mathbf{k}\uparrow}^{\dagger} c_{-\mathbf{k}\downarrow}^{\dagger} b_{\mathbf{q}} + b_{\mathbf{k}}^{\dagger} c_{-\mathbf{q}\downarrow} c_{\mathbf{q}\uparrow} - b_{\mathbf{k}}^{\dagger} b_{\mathbf{q}}). \tag{21}$$

We define a parameter, Δ that will later turn out to be the energy gap, just like before:

$$\Delta_{\mathbf{k}} = -\sum_{\mathbf{q}} V_{\mathbf{kq}} b_{\mathbf{q}}. \tag{22}$$

Introducing this into the Hamiltonian in Equation (21), we find it becomes:

$$\mathcal{H} = \sum_{\mathbf{k},s} \xi_{\mathbf{k}} c_{\mathbf{k},s}^{\dagger} c_{\mathbf{k},s} + \frac{1}{2} \sum_{\mathbf{k}} (\Delta_{\mathbf{k}} c_{\mathbf{k}\uparrow}^{\dagger} c_{-\mathbf{k}\downarrow}^{\dagger} + \Delta_{\mathbf{k}}^{*} c_{-\mathbf{q}\downarrow} c_{\mathbf{q}\uparrow} - \Delta_{\mathbf{k}} b_{\mathbf{k}}^{*}). \tag{23}$$

We define two new operators, $\gamma_{\mathbf{k}0}$ and $\gamma_{\mathbf{k}1}^{*}$ by the following:

$$c_{\mathbf{k}\uparrow} = u_{\mathbf{k}}^{*} \gamma_{\mathbf{k}0} + v_{\mathbf{k}} \gamma_{\mathbf{k}1}^{*}, \quad c_{-\mathbf{k}\downarrow}^{\dagger} = -v_{\mathbf{k}}^{*} \gamma_{\mathbf{k}0} + u_{\mathbf{k}} \gamma_{\mathbf{k}1}^{*}. \tag{24}$$

This is a Bogoliubov transformation, where $\gamma_{\mathbf{k}0}$ and $\gamma_{\mathbf{k}1}^{*}$ represent the creation and destruction of quasiparticles. Instead of working with the actual electrons, we have transformed into a state where we work with the quasiparticles, much like when we use center of mass coordinates in two-body problems, so that the algebra is easier. If you solve for the γ operators from Equation (24), we find that: $\gamma_{\mathbf{k}0} = u_{\mathbf{k}} c_{\mathbf{k}\uparrow} - v_{\mathbf{k}} c_{-\mathbf{k}\downarrow}^{\dagger}$. It is now easier to understand what the quasiparticle physically represents: an electron and a hole of negative momentum and opposite spin.

Substituting these into the Hamiltonian in Equation (23) and multiplying out the products we get terms involving $\gamma_{\mathbf{k}0}^{*}\gamma_{\mathbf{k}0}$, $\gamma_{\mathbf{k}1}^{*}\gamma_{\mathbf{k}1}$, $\gamma_{\mathbf{k}1}\gamma_{\mathbf{k}0}$ and $\gamma_{\mathbf{k}0}^{*}\gamma_{\mathbf{k}1}^{*}$. If we choose appropriate values of $u_{\mathbf{k}}$ and $v_{\mathbf{k}}$ so that the two cross terms, $\gamma_{\mathbf{k}1}\gamma_{\mathbf{k}0}$ and $\gamma_{\mathbf{k}0}^{*}\gamma_{\mathbf{k}1}^{*}$, vanish, then the Hamiltonian will be diagonalized. This is equivalent to solving Schrodinger equation. The condition for the two terms being zero is:

$$2\xi_{\mathbf{k}} u_{\mathbf{k}} v_{\mathbf{k}} + \Delta_{\mathbf{k}}^{*} v_{\mathbf{k}}^{2} - \Delta_{\mathbf{k}} u_{\mathbf{k}}^{2} = 0. \tag{25}$$

The solution to this quadractic equation is $\Delta_{\mathbf{k}}^{*} = (u_{\mathbf{k}}/v_{\mathbf{k}})(\sqrt{\xi_{\mathbf{k}}^{2} + |\Delta_{\mathbf{k}}|^{2}} - \xi_{\mathbf{k}})$. Since the total probablity is one, $|u_{\mathbf{k}}|^{2} + |v_{\mathbf{k}}|^{2} = 1$, we find the same result as we did earlier in Equation (17) – that is:

$$u_{\mathbf{k}}^{2} = \frac{1}{2}\left(1 + \frac{\xi_{\mathbf{k}}}{E_{\mathbf{k}}}\right), \qquad v_{\mathbf{k}}^{2} = \frac{1}{2}\left(1 - \frac{\xi_{\mathbf{k}}}{E_{\mathbf{k}}}\right). \tag{26}$$

Remebering that the cross terms, $\gamma_{\mathbf{k}1}\gamma_{\mathbf{k}0}$ and $\gamma_{\mathbf{k}0}^{*}\gamma_{\mathbf{k}1}^{*}$, are zero, if we substitute these values of $u_{\mathbf{k}}$ and $v_{\mathbf{k}}$ into the Hamiltonian (Equation (23)), we obtain this simplified Hamiltonian:

$$\mathcal{H} = \sum_{\mathbf{k}} (\xi_{\mathbf{k}} - E_{\mathbf{k}} + \Delta_{\mathbf{k}} b_{\mathbf{k}}^{*}) + \sum_{\mathbf{k}} E_{\mathbf{k}} (\gamma_{\mathbf{k}0}^{*}\gamma_{\mathbf{k}0} + \gamma_{\mathbf{k}1}^{*}\gamma_{\mathbf{k}1}). \tag{27}$$

This equation gives us a lot of insight into the energy of superconductivity. The first term gives us the energy of the ground state, and the second term gives us the energy of the excited quasiparticles (because it has the number operators $\gamma^*_{\mathbf{k}0}\gamma_{\mathbf{k}0}$ and $\gamma^*_{\mathbf{k}1}\gamma_{\mathbf{k}1}$ for the quasiparticles). It can easily be seen that $E_\mathbf{k}$ is the energy of one of these excited quasiparticles. Since $E_\mathbf{k} \equiv \sqrt{\xi^2_\mathbf{k} + |\Delta_\mathbf{k}|^2}$, the minimum energy required to create a quasiparticle (where $\xi_\mathbf{k} = 0$) is therefore $\Delta_\mathbf{k}$. This shows that $\Delta_\mathbf{k}$ really is the energy gap.

2.6 The Energy Gap

When we excite the superconductor with thermal energy, the quasiparticles are excited into various energy states, $E_\mathbf{k}$. Since the quasiparticles are fermions, they must obey Fermi-Dirac statistics which state the average occupation of the states, $\bar{n}_\mathbf{k}$. This is also the same as $\langle\gamma^*_\mathbf{k}\gamma_\mathbf{k}\rangle$ which is the number operator for the quasiparticle. Therefore we have the following, where β is the usual $1/kT$ [11, p.341]:

$$\langle\gamma^*_\mathbf{k}\gamma_\mathbf{k}\rangle = \bar{n}_\mathbf{k} = f(E_\mathbf{k}) = \frac{1}{e^{\beta E_\mathbf{k}} + 1}. \tag{28}$$

Recall our equation for $\Delta_\mathbf{k}$ in Equation (22). Again we make the simplification that $V_{\mathbf{kq}} = -V$ and $\Delta_\mathbf{k} = \Delta$. We can substitute γ operators for the c operators with, using Equation (24):

$$\Delta \;=\; V\sum_\mathbf{q}\langle c_{\mathbf{q}\uparrow}c_{-\mathbf{q}\downarrow}\rangle = V\sum_\mathbf{q}\langle(u^*_\mathbf{q}\gamma_{\mathbf{q}0} + v_\mathbf{q}\gamma^*_{\mathbf{q}1})(v^*_\mathbf{q}\gamma_{\mathbf{q}0} + u_\mathbf{q}\gamma^*_{\mathbf{q}1})\rangle. \tag{29}$$

Again we drop the cross terms, $\gamma_{\mathbf{q}0}\gamma^*_{\mathbf{q}1}$ and $\gamma^*_{\mathbf{q}1}\gamma_{\mathbf{q}0}$. Using the expectation values of the γ operators from Equation (28) and the values of $u_\mathbf{k}$ and $v_\mathbf{k}$ from Equation (17), we obtain:

$$\Delta \;=\; V\sum_\mathbf{q} u^*_\mathbf{q}v_\mathbf{q}\langle 1 - \gamma^*_{\mathbf{q}0}\gamma_{\mathbf{q}0} - \gamma^*_{\mathbf{q}1}\gamma_{\mathbf{q}1}\rangle, \tag{30}$$

$$\;=\; V\sum_\mathbf{q}\frac{\Delta}{2E_\mathbf{q}}(1 - 2f(E_\mathbf{q}), \tag{31}$$

$$\;=\; V\sum_\mathbf{q}\frac{\Delta}{2E_\mathbf{q}}\tanh\frac{\beta E_\mathbf{q}}{2}. \tag{32}$$

As before, we change the summation into an integral using the density of states and the Debye frequency cut-off. We arrive at a self-consistency condition that determines the energy gap:

$$\Delta = VN(0)\Delta\int_0^{\hbar\omega_D}\frac{\tanh\frac{1}{2}\beta\sqrt{\xi^2+\Delta^2}}{\sqrt{\xi^2+\Delta^2}}d\xi. \tag{33}$$

This is similar to the earlier derived one in Equation (19), except this one is valid at any temperature. In fact, putting in $T = 0$ it is trivial to see that it reduces down to the form in Equation (19).

At the critical temperature the energy gap of the superconductor is zero, because there is no energy difference between the two states; $\Delta(T_c) = 0$. The self-consistency equation in Equation (33) at this critical temperature then becomes: $VN(0)\int_0^{\hbar\omega_D}\tanh(\frac{1}{2}\beta\xi)/\xi d\xi = 1$. Evalauting this and solving for kT_c we find that $kT_c = 1.13\hbar\omega_D e^{-1/N(0)V}$. Recall our expression for the energy gap at zero temperature in Equation (20), $\Delta(0) = 2\hbar\omega_D e^{-1/N(0)V}$. Combining these two, we see:

$$\Delta(0) = 1.764kT_c. \tag{34}$$

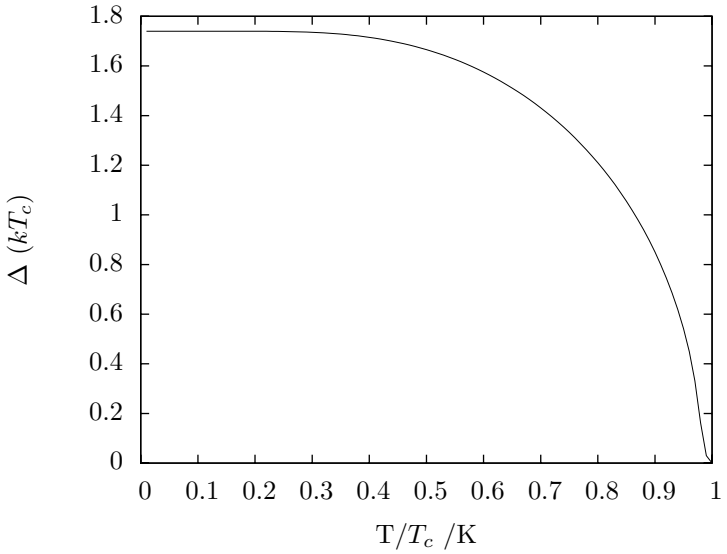

Figure 2: Δ plotted against temperature, expressed in units of kT_c, as given by Equation (34) and Equation (33). This was calculated by a numerical iterative method.

To actually calculate values for $\Delta(T)$ we need to use a numerical method, as the integral in Equation (33) has no explicit closed-form solution. We use an iterative method (see Listing 1) to calculate it: we choose a guess value for Δ, calculate the right hand side of Equation (33), and use this as the new value for Δ. This is repeated a few hundred times until the value is fairly constant. Figure 2 shows the curve of $\Delta(T)$.

2.7 Thermodynamic Quantities

We can now use standard statistical mechanical techniques to calculate various thermodynamic quantities. A couple of interesting properties that can be measured on superconductors are the heat capacity when in the superconducting state, C_s, and the free energy difference between the normal and supercondcting states, ΔF.

The entropy for the superconducting state is $S_s = -2k \sum_{\mathbf{k}} ((1-\bar{n}_{\mathbf{k}}) \ln(1-\bar{n}_{\mathbf{k}}) + \bar{n}_{\mathbf{k}} \ln \bar{n}_{\mathbf{k}})$, where $\bar{n}_{\mathbf{k}}$ is the average occupation of the $\mathbf{k}$ state, as given by Fermi–Dirac statistics in Equation (28). Again, we can turn the discrete sum into a continous integral over the velocity states by using the density of states. Additionally, $\bar{n}_{\mathbf{k}}$ becomes a function of ξ, i.e. $\bar{n}(\xi)$, and likewise $E_{\mathbf{k}}$ becomes $E(\xi)$. Therefore we have:

$$S_s = -2kN(0) \int_{-\infty}^{\infty} ((1-\bar{n}) \ln(1-\bar{n}) + \bar{n} \ln \bar{n})\, d\xi. \tag{35}$$

Knowing the entropy S_s we can then proceed to compute most thermodynamic quantities. One of the fundamental relations of thermodyanmics is:

$$dS = \frac{\delta Q}{T} = \frac{\delta Q}{dT} \frac{dT}{T} = C(T) \frac{dT}{T}. \tag{36}$$

In order to obtain the heat capacity $C(T)$, we can just divide both sides by dT/T to obtain:

$$\begin{aligned} C_s &= T\frac{dS_e}{dT} = -\beta\frac{dS_e}{d\beta}, && (37)\\ &= 2\beta k\int_{-\infty}^{\infty}\frac{\partial\bar{n}}{\partial\beta}\left(-\ln(1-\bar{n})+\ln\bar{n}\right)d\xi, && (38)\\ &= 2\beta k\int_{-\infty}^{\infty}\frac{\partial\bar{n}}{\partial\beta}\ln\left(\frac{\bar{n}}{1-\bar{n}}\right)d\xi = -2\beta^2 k\int_{-\infty}^{\infty}\frac{\partial\bar{n}}{\partial\beta}Ed\xi, && (39)\\ &= 2\beta k\int_{-\infty}^{\infty}-\frac{\partial\bar{n}}{\partial E}\left(E^2+\frac{1}{2}\beta\frac{d\Delta^2}{d\beta}\right)d\xi. && (40) \end{aligned}$$

For a normal metal, the electronic heat capacity is $C_n = \gamma T + AT^3$, where γ and A are constants that can be determined experimentally [11, p. 393]. Because we are dealing with very low temperatures, we can take the first order approximation and drop the T^3 term. The internal energy is simply the integral of the heat capacity: $U_n(T) = \int_0^T C_n dT = 0.5\gamma T^2$. From the fundamental thermodynamic relation in Equation (36), we see that $S_n(T) = \int_0^T C_n/T dT = \gamma T$. The free energy, $F = U - TS$, in the normal state is therefore:

$$F_n(T) = U_n(T) - TS_n(T) = -\frac{1}{2}\gamma T^2. \quad (41)$$

In our expression for $U_n(T)$ we implicitly assumed that the internal energy is zero at zero temperature, and this serves as our zero reference energy. When we calculate $U_s(T)$ we must be careful that there is no discontinuity in the energy at $T = T_c$ caused by choosing different reference energies. The easiest way to do this is start from $U_n(T_c)$ and calculate the difference by integrating the heat capacity C_s from T_c: $U_s(T) = U_n(T_c) - \int_T^{T_c} C_s dT = -\frac{1}{2}\gamma T_c^2 - \int_T^{T_c} C_s dT$. The free energy in the superconducting state is then:

$$F_s(T) = -\frac{1}{2}\gamma T_c^2 - \int_T^{T_c} C_s dT - TS_s(T), \quad (42)$$

where $S_s(T)$ is given in Equation (35), and C_s is in Equation (40).

What is often most interesting is the difference in free energy between the two states, as this determines the energy stability. Subtracting Equation (42) from Equation (41), we find:

$$\Delta F(T) = -\frac{1}{2}\gamma(T^2 + T_c^2) + \int_T^{T_c} C_s dT + TS_s(T). \quad (43)$$

3 Confirmation of BCS: Aluminium

Alumiunium is a standard well-understood superconductor, with a critical temperature of $T_c = 1.1793$ K and a critical field of $H_0 = 104.93$ G [6]. We will examine a couple of experimentally measured properties and see how these compare to the BCS predictions. Specifically, we will look at plots of the critical field H_c and the heat capacity C_s versus temperature.

3.1 Critical Field

Earlier we had derived an expression for the change in free energy between the superconducting state and the normal state, $\Delta F(T)$ in Equation (43). This difference is the reason why the material prefers to be in the lower energy superconducting state at these temperatures.

One of the phenomenons of superconductivity is that applied magnetic fields above a certain critical field destroy superconductivity and it reverts to being normal. The energy required to expel the magnetic field via the Meissner Effect is the usual energy of the magnetic field, $H^2/2\mu_0$. If this energy is greater than the free energy difference ΔF then the normal state is energetically preferable and superconductivity is lost. At the critical field value, H_c, we have:

$$H_c^2(T) \propto \Delta F = -\frac{1}{2}\gamma(T^2 + T_c^2) + \int_T^{T_c} C_s dT + TS_s(T). \tag{44}$$

Unfortunately this has no exact closed-form expression, because of the integral in C_s (Equation (40)) and $\Delta(T)$ in Equation (33), so we must compute this numerically (see Listing 1). Fortunately this is relatively easy as numerical integration is straightforward and we have explicit expressions for $\bar{n}$ and E. Calculation of $\Delta(T)$ is described earlier.

Figure 3 shows the critical field H_c of Aluminium. The overplotted line are the predictions as given by Equation (44). Various parameters in Equation (44) are not known, such as γ, but all these do is scale the graph in the horizontal and vertical directions. We set these as unity and scale the resulting graph by the critical temperature T_c and the critical field at absolute zero H_0. An oft-used empirical approximation is that $H_c \propto 1 - (T/T_c)^2$, so we plot that as a dotted line to provide a comparison.

It is immediately apparent that the predictions of the critical field from BCS theory seem to match the shape of the data quite well. Intriguingly it seems to deviate more in the middle of the temperature range, but at the high end (past 0.8 K) it is very accurate. Compared to the empirical relationship, BCS theory's predictions are much closer to the experimental data. On average BCS differed from the actual experimental data by 2%, but the empirical relationship differed by over 10%, clearly showing that BCS theory is more accurate.

3.2 Heat Capacity

A similar prediction of BCS theory is the heat capacity of the superconductor, C_s, in Equation (40). This also has been measured for a wide range of temperatures at both normal and superconducting states. Even though the temperature is below T_c, it can be forced to be normal by the use of a large magnetic field greater than H_c. Again a numerical integration is performed to get C_s (see Listing 1).

Figure 4 shows the two heat capacities at various temperatures. The overplotted line are the predictions as given by BCS theory in Equation (40) and the usual electronic heat capacity. We use the gradient of the normal heat capacity data to find γ, which can then be used to scale the predictions from Equation (40).

Again BCS theory predicts the general shape of the superconductor quite well, including the very well-known discontinuity jump in the heat capacity at $T = T_c$.

3.3 BCS Validity

Experiments involving quantum tunneling also provide evidence for BCS theory. More specifically, electron tunneling experiments seek to measure the energy gap directly. One experiment measured

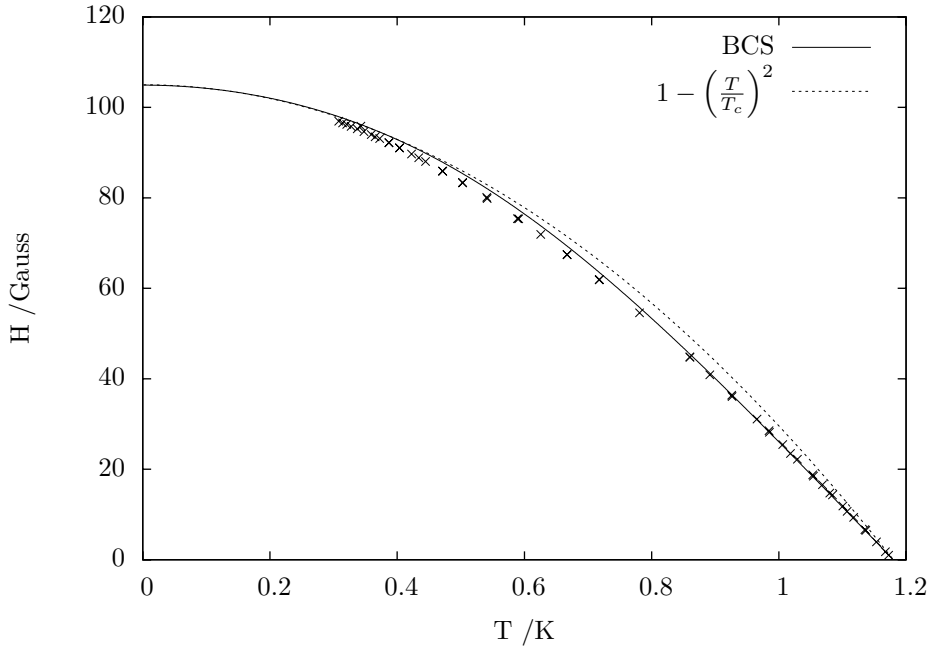

Figure 3: The critical field H_c of Aluminium ($T_c = 1.1793$ K and $H_0 = 104.93$ G) [6]. The overplotted line are the scaled predictions as given by Equation (44). The dotted line shows the predictions as given by the basic empirical relationship $1 - (T/T_c)^2$. The BCS theory predictions are significantly more accurate than the standard basic empirical relationship.

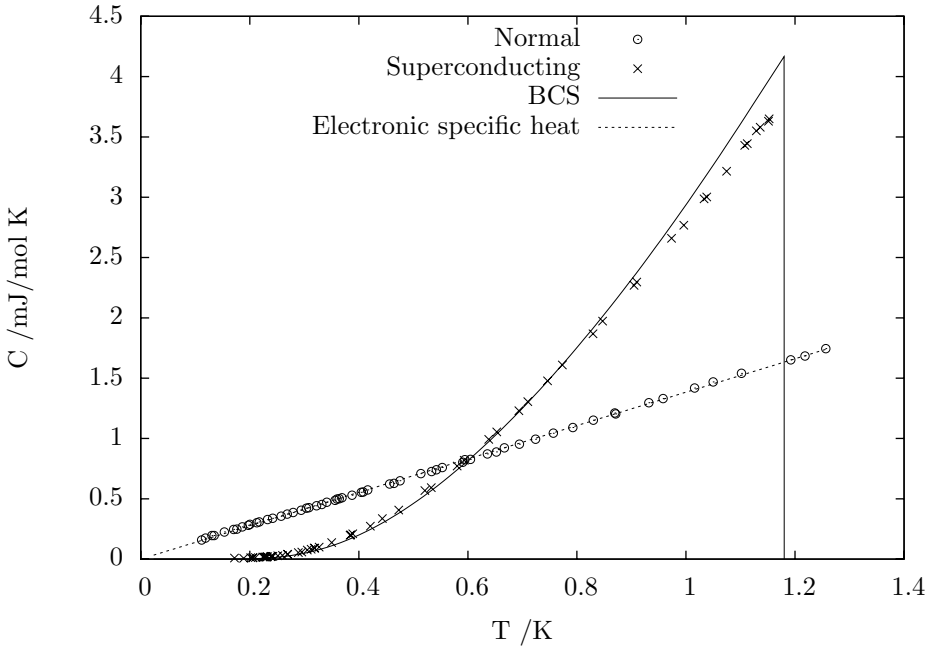

Figure 4: The heat capacity C of Aluminium ($T_c = 1.1793$ K) [10]. The overplotted line are the scaled predictions as given by Equation (40). The BCS theory predictions follow the curve of the data reasonably closely.

$2\Delta = (4.2 \pm 0.6)kT_c$ [5]. BCS from Equation (34) predicted that $2\Delta = 3.52kT_c$. This is just outside the quoted interval and is 1.13σ away from the BCS prediction. This is reasonable as the p-value for this is 13%, so this is still above the usual 5% significance level which would require us to reject our null hypothesis.

The critical field and the heat capacity as a function of temperature also seem to match the BCS theory predictions, along with the energy gap measured from tunelling experiments. Altogether these provide compelling evidence for the validity of the microscopic BCS theory for Aluminium.

4 Ginzburg-Landau Theory

4.1 Type I and Type II Superconductors

So far we have not mentioned any distinction between two different categories of superconductor: Type I and Type II. Aluminium used in our earlier section on validating BCS theory is a Type I superconductor. In these superconductors, as we mentioned earlier, the Meissner effect excludes magnetic fields from the bulk until the critical field is reached, at which point superconductivity collapses and it becomes completely normal.

On the other hand, Type II superconductors allow some penetration of the magnetic field. Up until the first critical field limit, H_{c1}, all the flux is excluded by the Meissner effect. After the second critical field limit, H_{c2}, supercondcutivity is lost. Between these two critical fields there is an intermediate state where some of the flux penetrates the bulk of the superconductor. This second order phase transition is the defining difference between Type I and Type II superconductors.

The microscopic BCS theory has no spatial dependence in any of the expressions for the ratio of superconducting charge carriers to normal state ones, $u_{\mathbf{k}}$ and $v_{\mathbf{k}}$. This poses problems for understanding Type II superconductors as the flux penetration causes spatial inhomogeneity. Instead we must look towards another theory.

4.2 The Ginzburg-Landau Equations

Ginzburg-Landau theory is a phenomological theory that attempts to explain superconductivity properties, without any references to the underlying microscopic quantum mechanical mechanisms. It begins by making an inspired guess at the free energy of a superconductor.

First of all, it introduces a variable, ψ, called the order parameter, which can be complex. The absolute value squared of the order parameter, $|\psi|^2$, represents the density of the superconducting charge carriers, n_s. This is similar to the quantum mechanical wavefunction. However, it is important to note that this is not quantum mechanical.

The fundamental postulate is that change in free energy between the superconducting state and the normal state, ΔF, is [13, p.111]:

$$\Delta F = \alpha|\psi|^2 + \frac{\beta}{2}|\psi|^4 + \frac{\hbar^2}{2m}\left|\left(\frac{\nabla}{i} - \frac{q}{\hbar}\mathbf{A}\right)\psi\right|^2 + \frac{H^2}{2\mu_0}. \tag{45}$$

If $\alpha < 0$ and $\beta > 0$, the first two terms create a quartic equation in $|\psi|$ where there are two minima. These correspond to the maximum superconducting charge carrier density where the energy is lowest. The third term contains the square of the gradient of the order parameter $|\nabla\psi|^2$ and this quantity is always positive. This expresses that any spatial inhomogeneity in the order parameter raises the energy and is unfavourable. Finally the last term, H^2, is the energy associated with the magnetic field. Experimental data shows m to be $2m_e$ and q to be $2e$ [13, p.114]. This corresponds with BCS theory's Cooper pairing, where two electrons form a bound charge carrying pair.

If $\beta > 0$, all the terms except the α term are positive. At temperatures below T_c, α must be negative in order for the superconducting free energy to be lower. However, at temperature above T_c, α must become positive so that the normal state free energy is always lower. We use the most simple expression for α: $\alpha(T) = -\alpha_0(1 - T/T_c)$.

Once again, we use a variational method, taking the derivative of Equation (45) with respect to ψ^*, finding:

$$\frac{\partial \Delta F}{\partial \psi^*} = \alpha\psi + 2\beta\psi\psi^*\psi + \frac{\hbar^2}{2m}\left|\frac{\nabla}{i} - \frac{q}{\hbar}\mathbf{A}\right|^2\psi = 0 \tag{46}$$

This is first Ginzburg-Landau Equation. The second Ginzburg-Landau Equation is also derived from Equation (45), except instead of varying ψ^*, $\mathbf{A}$ is varied instead. Since we do not need the second equation we will not derive it here.

4.3 Penetration Depth

The Meissner effect excludes magnetic flux from the superconductor bulk but some flux still penetrates near the surface, and it falls off the deeper we go. We can use the London equations (the most basic empirical theory of superconductivity) to model this.

If we take the second London equation, $\mathbf{H} = -\nabla\times((m/n_s e^2)\mathbf{J}_s)$, and take the curl of Maxwell's equation, $\nabla \times \mathbf{h} = \mu_0\mathbf{J}$, we find: $\nabla^2\mathbf{H} = (n_s e^2\mu_0/m)\mathbf{H}$ [13, p.4]. This differential equation has the

usual decaying exponential solution, $H(x) = H_0 e^{-x/\lambda}$, where λ is defined by:

$$\lambda^2 = \frac{n_s e^2 \mu_0}{m}. \tag{47}$$

It is worth noting that in our Ginzburg-Landau framework, n_s is the same as $|\psi_\infty|^2$, the maximum value of superconducting carrier density. The λ in this exponential decay is a length constant which determines the rate of the fall-off with distance, which we call the penetration depth.

4.4 Coherence Length

Deep inside the superconductor, the free energy reaches the minimum value when (this can be seen by taking the derivative of Equation (45) with respect to $|\psi|^2$):

$$|\psi_\infty|^2 = \frac{\alpha}{\beta}. \tag{48}$$

If we take a situation where there are no magnetic fields present, in other words $\mathbf{A} = 0$, and if we assume that ψ is real, then we find Equation (46) reduces to the following in one dimension:

$$\alpha\psi + 2\beta\psi^3 + \frac{\hbar^2}{2m}\frac{d^2\psi}{dx^2} = 0. \tag{49}$$

If we choose the situation such that $x < 0$ is normal and $x > 0$ is superconducting, with the phase transition on the boundary $x = 0$, then we find the solution to this differential equation is:

$$\psi(x) = \psi_\infty \tanh\frac{x}{\sqrt{2}\xi}, \tag{50}$$

where

$$\xi(T)^2 = \frac{\hbar^2}{2m|\alpha(T)|}. \tag{51}$$

This ξ is clearly a length, and so we call it the characteristic length. Equation (50) describes how the amount of superconducting charge carriers gradually increases from zero to the maximum value, ψ_∞, over a distance determined by ξ, as you cross the boundary from a normal region to a superconducting one.

If we look at the simplest situation where we have no fields or gradients, we can substitute Equation (48) back into our expression for ΔF in Equation (45). The energy difference ΔF is related to the thermodynamic critical field, as it is the energy used to expel the flux. Therefore we find:

$$\frac{H_c^2}{\mu_0} = -\frac{\alpha^2}{\beta}. \tag{52}$$

Solving Equation (47), Equation (48) and Equation (52), we obtain an expression that links α with λ and H_c: $\alpha = -(4\pi q^2/m)H_c^2\lambda^2$. This can now be substitued into Equation (51) to yield:

$$\xi(T) = \frac{\hbar}{\sqrt{2}qH_c\lambda}. \tag{53}$$

Both ξ and λ turn out to be very important coeffecients that summarise the state of the superconductor in the Ginzburg-Landau framework. We define a parameter κ which is called the Ginzburg-Landau parameter:

$$\kappa \equiv \frac{\lambda(T)}{\xi(T)} = \frac{\sqrt{2}qH_c\lambda^2}{\hbar}. \tag{54}$$

This ratio between the coherence length and the penetration depth encapsulates whether a superconductor has Type I or Type II behaviour. Superconductors with small κ (large coherence length and small penetration depth) are Type I, and conversely those with a large κ are Type II.

To understand this we refer to a qualitative energetic argument based off Equation (45). It costs energy to exclude the magnetic flux ($H^2/2\mu_0$), so allowing some to penetrate is desirable. However, allowing the magnetic field to penetrate lowers the superconducting charge carrier density ($|\psi|^2$) near the surface, which is energetically undesirable.

With a small κ, the magnetic field does not penetrate very far due to the small penetration depth, saving very little energy, whilst the superconducting charge carrier density is affected much more due to the large coherence length, incurring a very large energy cost. Overall, the superconductor does not like forming superconducting–normal boundaries as the energy actually increases.

On the other hand, for one with a large κ the opposite occurs: the magnetic field penetrates lots incurring significant energy savings and the carrier density is not affected much incurring little energy cost. Overall, it prefers to form superconducting–normal boundaries; the flux penetrates the bulk of the superconductor and forms vortices where the middle of these are normal and allow the flux to penetrate, whilst surrounding them are supercurrents screening the flux from the rest of the superconductor [13, p.143]. This is known as nucleation or the Arbikosov vortex state.

Figure 5 shows pictorially this argument, where the area under the curves (shaded in grey) represent either energy losses or gains. The parameters ξ and λ are shown to measure the lengths at which the fall-off and penetration respectively occur. It is clear that for Type I it costs energy to form a boundary, but for Type II it saves energy.

4.5 Upper critical field

We wish to find the upper critical field in a bulk sample. Again this derivation follows that given in Tinkham [13, p.134]. Let us put the applied magnetic field H_{c2} along the z axis, and our vector potential could be $\mathbf{A} = H_{c2}x\ \hat{y}$. Now we put this into the Ginzburg-Landau equation and find the largest value of H_{c2} for which non-trivial solutions exist. To simplify things, we linearize the Ginzburg-Landau equation from Equation (46), by dropping the $\psi\psi^*\psi$ term. Altogether this leaves us with:

$$\alpha\psi + \frac{\hbar^2}{2m}\left|\frac{\nabla}{i} - \frac{q}{\hbar}H_{c2}x\hat{y}\right|^2\psi = 0, \tag{55}$$

$$\left(-\nabla^2 + \frac{2qi}{\hbar}H_{c2}x\frac{\partial}{\partial y} + \frac{q^2}{\hbar^2}H_{c2}^2x^2\right)\psi = -\frac{2m}{\hbar^2}\alpha\psi. \tag{56}$$

For our ansantz, we seek a ψ where the variables are seperated, i.e. $\psi = X(x)Y(y)Z(z)$. The potential $\mathbf{A}$ is only dependent on x and not y nor z, so it seems reasonable to let $Y(y) = e^{ik_y y}$ and $Z(z) = e^{ik_z z}$, the usual phasors. We then set $X(x) = f(x)$ for notational simplicity. The ansantz therefore is:

$$\psi = e^{ik_y y}e^{ik_z z}f(x). \tag{57}$$

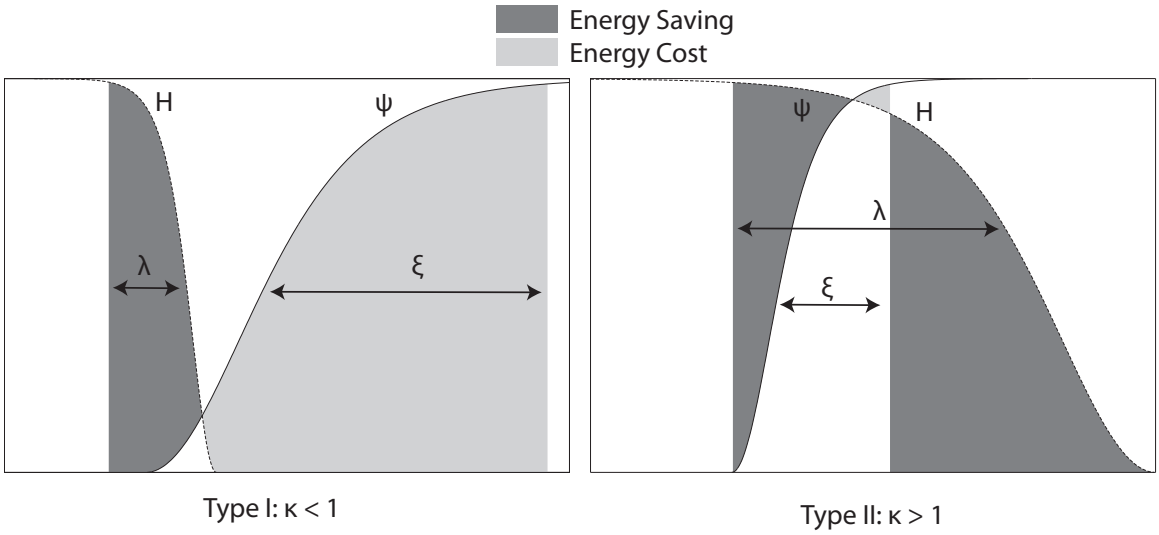

Figure 5: A diagram showing the order parameter and the magnetic field at a normal-superconducting boundary. The parameters ξ and λ are shown to measure the lengths at which the fall-off and penetration respectively occur. The shaded areas under the curves represent energy losses or gains. It is clear that Type I does not prefer to make boundaries but Type II does, explaining the flux penetration.

Substituting this into the linear Ginzburg-Landau equation, Equation (56), dividing both sides by $e^{ik_y y}$ and $e^{ik_z z}$ and multiplying both sides by $\hbar^2/2m$, we find:

$$-\frac{\hbar^2}{2m}f'' + \frac{1}{2}m\left(\frac{qH_{c2}}{m}\right)^2\left(x - \frac{\hbar}{qH_{c2}}k_y\right)^2 f \quad = \quad \frac{\hbar^2}{2m}\left(\frac{1}{\xi^2} - k_z^2\right)f. \tag{58}$$

The Schrodinger equation for a particle in an oscillator potential in one dimension has the form $-(\hbar/2m)\psi'' + \frac{1}{2}m\omega^2 x^2\psi = E\psi$. If this is solved, one finds the possible energy eigenvalues are quantized in levels given by $E = (n + \frac{1}{2})\hbar\omega$. Equation (58) has a form very similar to that of the quantum harmonic oscillator, only with $E = (\hbar^2/2m)(\xi^{-2} - k_z^2)$ and $\omega = qH_{c2}/m$. If we put these into our equation for the energy eigenvalues we find:

$$\left(n + \frac{1}{2}\right)\hbar\frac{qH_{c2}}{m} = \frac{\hbar^2}{2m}\left(\frac{1}{\xi^2} - k_z^2\right). \tag{59}$$

Rearranging for H_{c2}:

$$H_{c2} = \frac{\hbar}{2q(n + \frac{1}{2})}\left(\frac{1}{\xi^2} - k_z^2\right). \tag{60}$$

This is a maximum when $n = 0$ and $k_z = 0$. Therefore we find the upper critical field is:

$$H_{c2} = \frac{\hbar}{q}\frac{1}{\xi^2}. \tag{61}$$

Recall κ from Equation (54). If we arrange it, we have:

$$H_{c2} \quad = \quad \frac{\hbar}{q}\frac{\kappa^2}{\lambda^2} = \frac{\hbar}{q}\frac{2q^2H_c^2\lambda^2}{\hbar^2}, \tag{62}$$

$$\quad = \quad \sqrt{2}\kappa H_c \tag{63}$$

Here we see that κ relates the upper critical field H_{c2} to the thermodynamic critical field H_c. This is the link between the earlier BCS theory for Type I superconductors, where we derived an expression for H_c in Equation (44), and the Ginzburg-Landau theory of Type II superconductors with their upper critical field. It is obvious that Equation (63) shows that $\kappa = 1/\sqrt{2}$ is the critical value at which Type I turns into Type II behvaiour, because if $\kappa > 1/\sqrt{2}$ then $H_{c2} > H_c$, and if $\kappa < 1/\sqrt{2}$ then $H_{c2} < H_c$.

5 Magnesium Diboride

Magnesium diboride (MgB_2) is a recently discovered Type II superconductor that has garnered much interest because of its high critical temperature ($T_c = 39$ K). Since it is relatively new, a consensus on whether it can be classified as a conventional BCS superconductor or not has not yet been reached. We shall use BCS theory, as derived earlier, to investigate MgB_2. Once again we will look at the critical field and heat capacity as a function of temperature.

5.1 Upper Critical Field

Figure 6 shows H_{c2} plotted against temperature for MgB_2. The overplotted line are the predictions as given by standard BCS theory for H_c from Equation (44), scaled by T_c and H_0. It is immediately apparent that the shape of H_{c2} in Figure 6 is very different from the shape of H_c as shown in Figure 3. Whilst the BCS theory predictions for Aluminium worked well, for MgB_2 it does not seem too accurate.

This deviation between experimental data and theory predictions is perhaps due to the various approximations we have made in our derivation of BCS theory. We assumed that the scattering potential was constant for all momentum states, i.e. $V_{\mathbf{kq}} = -V$, and that the Fermi surface for the electrons was perfectly spherical. These approximations might not be particularly accurate, especially when considering a complex compound like MgB_2.

5.2 Heat Capacity

Again we look at the heat capacity, which is predicted by BCS theory in Equation (40). Instead of plotting the heat capacities of the normal and superconducting states on the same graph like we did in Figure 4, we plot the difference in heat capacity between the superconducting and normal states divided by the temperature, $(C_s - C_n)/T$. This is done because it makes it easier to see the deviations of the experimental data from the theory, especially at low temperatures.

Figure 7 shows the result of this plotting. The overplotted line are the predictions as given by BCS theory for $(C_s - C_n)/T$, using Equation (40) and $C_n = \gamma T$. Again these were scaled. In this case T_c scaled it horizontally and an arbitary constant was used to scale it vertically.

BCS theory performs very well at the medium and high end of the temperature scale, where it follows the experimental data quite well. Right at the peak around 34 K there is a noticeable deviation: the expeirmental has quite a rounded peak and the fall-off near T_c is not vertical. On the other hand BCS predicts a very sharp corner with the characteristic discontuinity in heat capacity.

This is perhaps because impurities in the MgB_2 sample might cause cause the sample to be not uniform. For example, some macroscopic bulk of the sample might be normal and some parts might be superconducting at the same time, and so the horizontal resolution of the data is diminished and the peak becomes wider and less sharp.

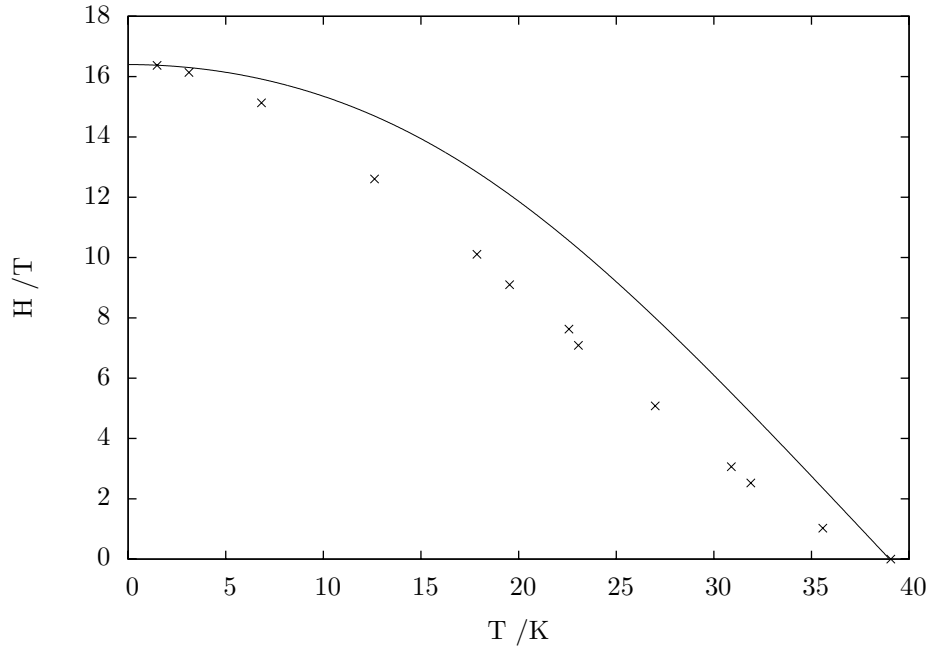

Figure 6: The upper critical field H_{c2} of MgB_2 ($T_c \approx 39$ K and $H_0 \approx 16.4$ T) [2]. The dotted line are the predictions as given by standard BCS theory for H_c from Equation (44). The deviations are perhaps attributable to approximations in BCS theory.

The low temperature region below 10 K is intriguing though and does not seem to match our BCS predictions at all. Not only does it continue to fall whilst the BCS prediction levels off, it falls at an even faster rate, before starting to level off around 2–3 K. This is a pretty significant deviation and suggests that something is wrong with our BCS theory model. One thing that has been suggested is that this is evidence of the presence of two energy gaps, where as BCS theory traditionally only has the one gap [14]. In the next section we investigate this idea, by extending our BCS theory to account for two gaps.

5.3 Two Energy Gaps

Recall that BCS theory in Equation (34) related the energy gap $\Delta(0)$ to some multiple of kT_c, specifically that the energy gap was approximately $3.5kT_c$. This was derived using many approximations; perhaps most significantly we used a constant potential for all the electron-phonon interactions, which neglects to take into account anything specific about the material. It seems plausible that different materials might have a different energy gap.

Here we deviate from the usual BCS treatment and specify two energy gaps, each with different energies. For a superconductor with two energy gaps we perform the heat capacity calculations of Equation (40) twice, once for each energy gap. The two heat capacities then are simply added in some linear combination [8]:

$$C_s = KC_{s1} + (1 - K)C_{s2} \tag{64}$$

Although we could use data from tunneling experiments for the energy gaps, there seems to

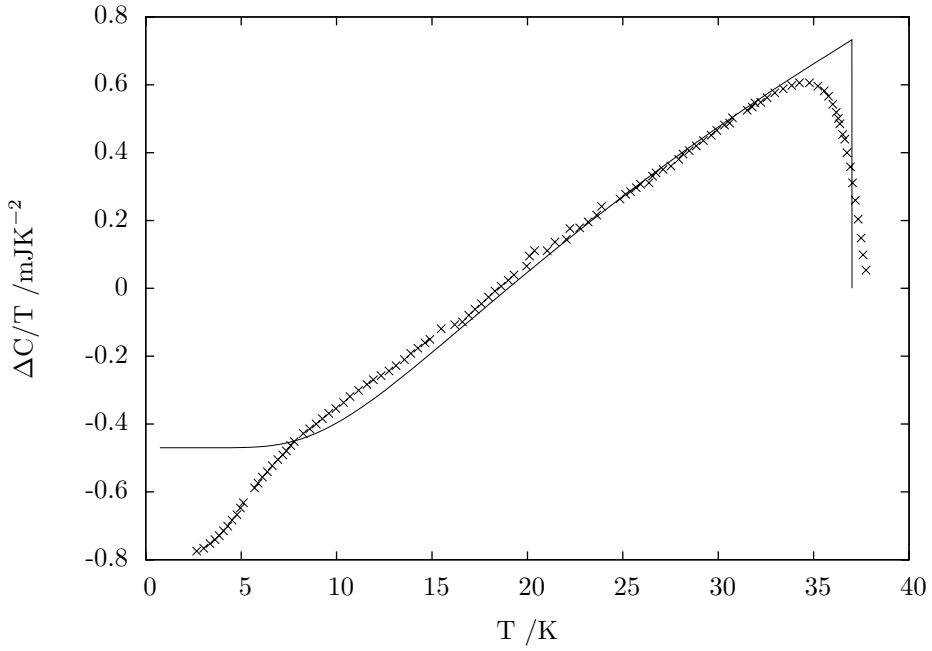

Figure 7: The difference in heat capacity between the superconducting and normal states divided by the temperature for MgB_2, i.e. $(C_s - C_n)/T$ [14]. The overplotted line are the predictions as given by BCS theory for $(C_s - C_n)/T$, using Equation (40) and $C_n = \gamma T$. It seems accurate for high temperatures, but is rather poor below 10 K.

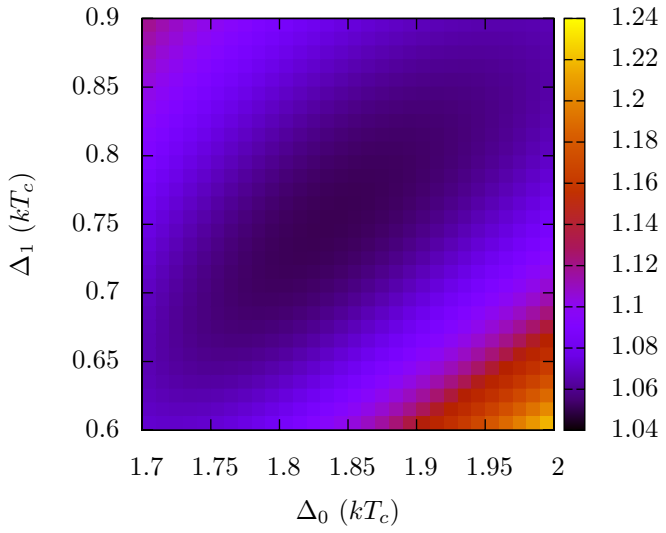

Figure 8: A contour plot showing the deviation from the data with respect to the two energy gap values, Δ_0 and Δ_1 [14]. Lower values are better. It seems like the optimum values lie in the middle around $\Delta_0 = 1.85\ kT_c$ and $\Delta_1 = 0.75\ kT_c$.

be a wide range of values that have been calculated and they do not seem that accurate or reliable. Instead we seek to find our own estimates for the energy gaps, by comparing our predictions with actual experimental data for MgB_2. The exact procedure we followed is outlined below (see Listing 1 for the code):

First of all, we choose a pair of values for the enegy gaps. We proceed to compute C_{s1} and C_{s2} for these. We then use a standard numerical minimization algorithm to minimize an error metric, E, by varying K, the ratio between the two gap's contribution, and A, an overall scaling factor. The error metric is the usual least-squared deviation from the actual data points, O_i, as given by:

$$E = \sum_i \left(A \frac{K C_{s1}(T_i) + (1-K) C_{s2}(T_i) - \gamma T_i}{T_i} - O_i \right). \tag{65}$$

We record the lowest E we could achieve for those two energy gap values. Finally we repeat this process with a range of values for the energy gaps, so that we can investiagate which energy gaps match our data best. For this we used the range: $1.1\ kT_c \leq \Delta_1 \leq 3.0\ kT_c$ and $0.1\ kT_c \leq \Delta_2 \leq 1.0\ kT_c$.

Figure 8 is a contour map showing the lowest error metric we could obtain for that pair of energy gap values. On the x axis is Δ_1 and on the y axis is Δ_2, in units of kT_c. The optimum values seems to be in the middle of Figure 8 around $\Delta_0 = 1.85\ kT_c$ and $\Delta_1 = 0.75\ kT_c$.

We then ran the procedure again, but with smaller steps of energy gap values around the central region mentioned above, to obtain better resolution. Taking the lowest error result, the

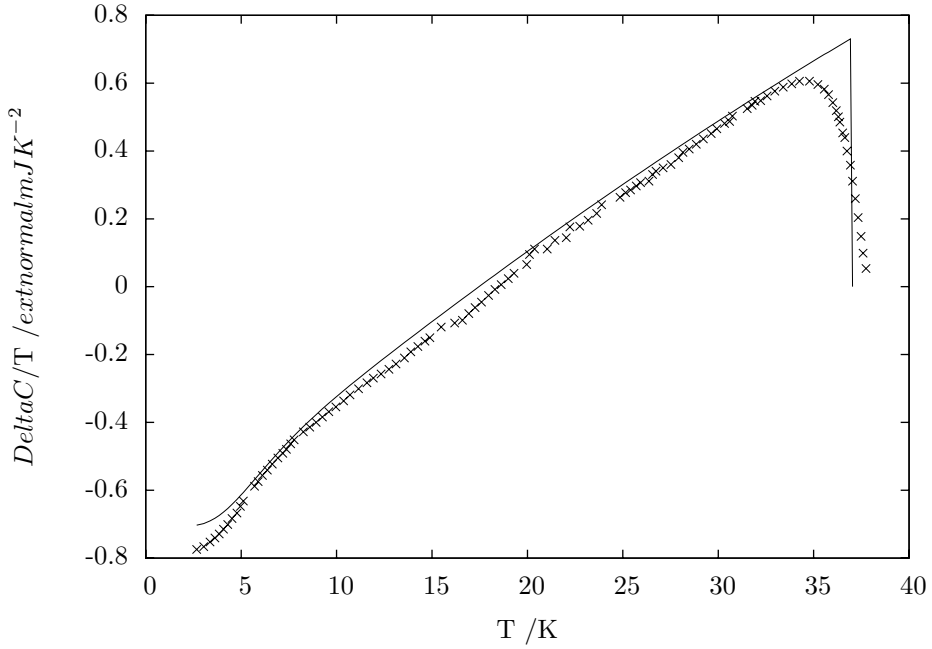

Figure 9: The difference in heat capacity between the superconducting and normal states divided by the temperature for MgB_2, i.e. $(C_s - C_n)/T$[14]. The overplotted line are the predictions as given by our multi-gap model for $(C_s - C_n)/T$, using Equation (64) and $C_n = \gamma T$. The energy gaps used are our best estimates: $\Delta_1 = 1.84\ kT_c$ and $\Delta_2 = 0.75\ kT_c$. This two gap model is much better than our earlier one gap model in Figure 7.

energy gap values here form our best estimates for the energy gap:

$$\Delta_1 = 1.84\ kT_c, \qquad \Delta_2 = 0.75\ kT_c. \tag{66}$$

Figure 9 shows the results of our two gap heat capacity model using the energy gaps in Equation (66), overplotted on top of the actual experimental data. It retains the earlier good fit at high temperatures in Figure 7, but it now also matches the low temperature range much better than before. It no longer levels out at 10 K, but falls at an even faster rate before levelling off around 2 K. This matches our experimental data better than in Figure 7, which was when we were using standard BCS theory.

The larger energy gap ($\Delta_0 = 1.84\ kT_c$) dominates the high temperature region like we had in Figure 7 for the one-gap model. The smaller energy gap ($\Delta_1 = 0.75\ kT_c$) introduces the low temperature behaviour where the larger gap does not have any contribution to the heat capacity. To get the best fit, we found that $K \approx 0.53$. This indicates that the smaller energy gap and the larger energy gap are approximately equally abundant and contribute to the heat capacity equally.

This two gap model is a huge improvement over the one gap model and gives up strong evidence that MgB_2 can not be treated as an ideal BCS superconductor and there might perhaps be two energy gaps. The two energy gaps arise from the different electron bands in the material.

The structure of MgB_2 is layered: the boron atoms form a hexagonal planar layer and the magnesium ions sit in a plane between two layers of boron, as seen in Figure 10 [3]. The boron atoms are bonded covalently with σ bonds, but the hexagonal rings also create π bonds above and

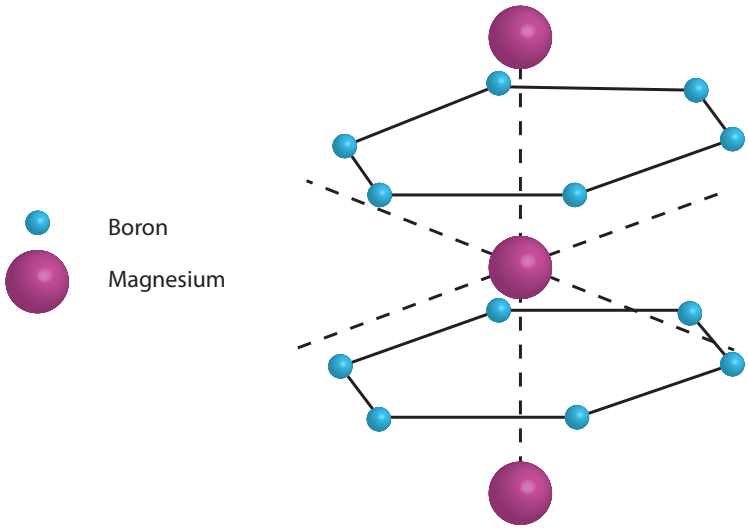

Figure 10: The crystal lattice structure of MgB_2 [3]. The hexagonal boron layers have both π and σ bonds that cause the two energy gap superconductivity.

below the plane. The electrons that form the Cooper pair can come from either the σ bonds or the π bonds, and the energy gap for each of these are different. This gives rise to the two energy gaps that we have seen in MgB_2 superconductivity.

6 Conclusion

Experiments involving electron tunneling in MgB_2 have suggested energy gaps of $\Delta_1 = 6$–7 meV and $\Delta_2 = 1$–2 meV [12]. Our best estimates are $\Delta_1 = 5.85$ meV and $\Delta_2 = 2.4$ meV, which are not too far off those derived from tunnelling. This confirms that our values for the energy gaps seem plausible, and in turn this suggests that our adapted BCS theory is correct.

It seems unambigious that MgB_2 has multiple energy gaps, as standard BCS theory with a single gap cannot fully describe the heat capacity. Two energy gaps appears to be sufficient to describe the behaviour. Apart from the double energy gap, MgB_2 seems to behave like a conventional superconductor, as, with the gap correction, the heat capacity matched our theoretical predictions well. This is unlike high-temeperature superconductors, such as YBCO, which are unconventional superconductors.

Mathematica Code

```
k = 1
grand[x_, d_, T_] := d Tanh[1/2 1/(k T) (x^2 + d^2)^(1/2)]/(x^2 + d^2)^(1/2)
delta0 = Last[NestList[NIntegrate[#  1/(x^2 + #^2)^(1/2), {x, 0, 5}] &, 1, 300]]
delta[T_, gap_] := delta[T, gap] = gap*Last[NestList[
        NIntegrate[grand[x, #, T*2.27], {x, 0, 5}] &, 1, 300]]/delta0;
energy[T_, x_, gap_] := energy[T, x, gap] = Sqrt[delta[T, gap]^2 + x^2];
f[T_, x_, gap_] := ff[T, x, gap] = (1 + Exp[energy[T, x, gap]/(k T)])^-1;
ff[T_, x_, gap_] := ff[T, x, gap] = -(1 + Exp[energy[T, x, gap]/(k T)])^
```

```
9         -2 Exp[energy[T, x, gap]/(k T)] 1/(k T);
10 dd[T_, gap_] := dd[T, gap] = (delta[T + 0.001, gap]^2 - delta[T - 0.001, gap]^2)
11         /0.002;
12 Cs[T_, gap_] := Cs[T, gap] = 2/(k T) NIntegrate[-ff[T, x, gap]
13         (energy[T, x, gap]^2 - 1/2 T dd[T, gap]), {x, -Infinity, Infinity},
14         PrecisionGoal -> 8 ];
15 gam = 2 Pi Pi/3;
16
17 bcsgap = 1.76
18 Tc = 1
19 Se[T_] := -2 k NIntegrate[(1 - f[T, x, bcsgap]) Log[1 - f[T, x, bcsgap]] +
20     f[T, x, bcsgap] Log[f[T, x]], {x, -Infinity, Infinity},
21    PrecisionGoal -> 8 ]
22 DF[T_] := -(1/2) gam T^2 - (1/2 gam Tc^2 -
23      NIntegrate[Cs[T2, bcsgap], {T2, T, Tc}, PrecisionGoal -> 8 ] - T Se[T]);
24
25 data = Import["mgb2-cs-mathematica.csv"];
26 dc = Map[Last, data]; temps = Map[First, data]/37;
27 pred[a_, c_, g1_, g2_] := c ((a Table[Cs[t, g1], {t, temps}] +
28         (1 - a) Table[Cs[t, g2], {t, temps}])/gam/temps - 1);
29 error[g_] := {g, First[NMinimize[{Total[(pred[a, c, First[g], Last[g]] - dc)^2]},
30         {a,c}]]}
31 contourplot = Map[error, Tuples[{Range[1.1, 3.0, 0.3], Range[0.1, 1.0, 0.3]}]]
```

Listing 1: The Mathematica code used for generating $\Delta(T)$, $C_s(T)$ and $H_c(T)$, as well as finding the two energy gaps for MgB_2.

Some notes on the the code:

- Most functions take a user-specified gap in units of kT_c. For example, for conventional BCS theory this would be 1.74.
- $x \equiv \xi$
- Line 4: $\Delta(T)$, in units of kT_c.
- Line 7: $\bar{n}$
- Line 8: $\frac{d\bar{n}}{dE}$
- Line 10: $\frac{d\Delta}{dT}$
- Line 19: $S_s(T)$
- Line 22: $\Delta F(T)$
- Line 27–31: Functions used for trying different energy gaps, performing the minimization and calculating the deviation from the experimental data

References

[1] Stephen Blundell, *Superconductivity: A very short introduction.* (New York: Oxford University Press, 2009).

[2] Cristina Buzea and Tsutomu Yamashita, "Review of the superconducting properties of MgB_2," *Supercond. Sci. Technol.* 14 (2001) R115–R146.

[3] Hyoung Joon Choi *et al.*, "The origin of the anomalous superconducting properties of MgB_2", *Nature* 418 (2002), 758-60.

[4] Leon N. Cooper, "Bound Electron Pairs in a Degenerate Fermi Gas", *Physical Review* 104 (1956), 1189–1190.

[5] Ivar Giaever and Karl Megerle, "Study of Superconductors by Electron Tunneling," *Physical Review* 122 (1961): 1101–1111.

[6] E. P. Haris and D. E. Mapother, "Critical Field of Superconducting Aluminum as a Function of Pressure and Temperature above 0.3 K," *Physical Review* 165 (1968), 522–532.

[7] Emanuel Maxwell, "Isotope Effect in the Superconductivity of Mercury", *Physical Review* 78 (1950), 477.

[8] Y. Nakajima, T. Nakagawa, T. Tamegai and H. Harima, "Specific-Heat Evidence for Two-Gap Superconductivity in the Ternary-Iron Silicide $Lu_2Fe_3Si_5$," *Physical Review Letters* 100, 157001 (2008).

[9] N. P. Ong, Superconductivity II. Princeton University (2001).

[10] Norman E. Phillips, "Heat Capacity of Aluminum between 0.1K and 4K," *Physical Review* 114 (1959): 676–685.

[11] F. Reif, *Fundamentals of Statistical and Thermal Physics.* (Illinois: Waveland Press, 1965).

[12] S. Souma *et al.*, "The origin of multiple superconducting gaps in MgB2", *Nature* 423 (2003), 65-67.

[13] Michael Tinkham, *Introduction to Superconductivity.* (New York: Dover Publications, 2nd Edition, 2004).

[14] Yuxing Wang, Tomasz Plackowski, Alain Junod, "Specific heat in the superconducting and normal state (2–300 K, 0–16T), and magnetic susceptibility of the 38 K superconductor MgB_2: evidence for a multi component gap," *Physica C* 355 (2001): 179–193.